

# Preparation of Fe-doped TiO<sub>2</sub> nanotube and their photocatalytic activity

C. KANG<sup>a\*</sup>, B. DU<sup>a</sup>, Z. YANG<sup>a</sup>, E. XIE<sup>b</sup>

<sup>a</sup>*Nonlinear Research Institute, Baoji University of Arts and Sciences, Baoji 721016, China*

<sup>b</sup>*School of Physical Science and Technology, Lanzhou University, Lanzhou 730000, China*

Fe-doped TiO<sub>2</sub> nanotubes were prepared by anodization and solution-coating technique. Field-emission scanning electron microscopy (SEM) and transmission electron microscope (TEM) were employed to characterize the morphology and structure of the nanotubes. The photocatalytic performance of Fe-doped TiO<sub>2</sub> nanotube was indicated by photo-decomposition rate of Rhodamine B under ultraviolet-visible light irradiation. The results show that Fe-doped TiO<sub>2</sub> nanotubes with the optimal concentration exhibit excellent photocatalytic activity compared to the undoped TiO<sub>2</sub> nanotubes and the nanotubes with excessive Fe-doped proportion. This could be explained as Fe ions may play a role as e<sup>-</sup> or h<sup>+</sup> traps and reduces e<sup>-</sup>/h<sup>+</sup> pair recombination rate and thus improves photocatalytic efficiency. However, excessive Fe ions decrease photocatalytic efficiency immensely.

(Received February 3, 2015; accepted September 9, 2015)

**Keywords:** TiO<sub>2</sub> nanotube; Anodization; Fe-doped; Photocatalytic

## 1. Introduction

TiO<sub>2</sub> nanomaterials have attracted increasingly interest due to their larger specific surface areas, non-toxicity, biological compatibility, and low cost [1-3]. Especially for nanotube, it offering a large internal surface area and faster electron transport capability, possesses greater potential using in photocatalytic decomposition of organic pollutants, high-efficiency dye sensitized solar cells and biological organ transplant etc. [4-6]. In recent years, various of synthetic routes such as hydrothermal technology, electrospinning, and anodization have been explored for all kinds of inorganic material nanotube [7-10]. Among them, anodization synthesis is a simple and controllable method for massive producing oriented and high length-diameter ratio TiO<sub>2</sub> nanotubes [11-13].

With the continuous improvements of the process of industrialization and the people's gradual rising environmental protection consciousness, processing pollutants in a safe and efficient way become more and more essential for further development of the industry. Among various methods for decomposition of pollutants, photocatalytic decomposition is a high-efficiency and energy-saving way. TiO<sub>2</sub> nanomaterials have been proved to be the most preferable environmentally friendly photocatalyst because of its high oxidative power, stability, low cost and non-toxicity and can be applied in eliminating persistent organic pollutants in water [14-16]. However, this type of photocatalyst is only effective under ultraviolet irradiation ( $\lambda < 380$  nm) due to its large band gap (3.2eV), which cover about 4% energy of the full solar

spectrum [17, 18]. Accordingly, improving photocatalytic efficiency of TiO<sub>2</sub> materials by extending its optical response into visible range has been studied extensively [19, 20]. Doping Fe is a promising method to adjust TiO<sub>2</sub> band gap [21].

In our work, TiO<sub>2</sub> nanotubes were prepared by anodization and were doped different percents of Fe-ions on the surface of TiO<sub>2</sub> nanotubes. The photocatalytic properties of these types of nanotubes with different Fe-doped amounts were studied.

## 2. Experimental

### 2.1. Preparation of Fe-doped TiO<sub>2</sub> nanotube

TiO<sub>2</sub> nanotubes were synthesized by potentiostatic anodization in a two-electrode electrochemical system. A potentiostatic direct-current (DC) power supply was applied as impetus appliance with a cleaned Ti foil as photoanode and a Ti sheet as photocathode. The electrolyte consists of a 0.25 wt% NH<sub>4</sub>F contained ethylene glycol solution with 2 vol% H<sub>2</sub>O added. The anodization process was conducted at a voltage of 50V with a weak current of 50mA for 24h. After anodization, we obtained an oriented nanotube membrane. Then the membrane was treated to peel off from the substrate. Subsequently, the membrane was grinded in an agate mortar for about 30min to obtain a uniform powder. Fe-doped nanotube powers were obtained by immersing the powers in 10mL aqueous solution containing 0.05g,

0.1g, 0.2g Fe(NO<sub>3</sub>)<sub>3</sub>, respectively. The unprocessed TiO<sub>2</sub> nanotube power was also retained as a comparison. Then all the powers were sintered at 550°C for 3h in air. The four samples were marked as Fe-0.05-TiO<sub>2</sub>, Fe-0.1-TiO<sub>2</sub>, Fe-0.2-TiO<sub>2</sub>, undoped TiO<sub>2</sub>, respectively.

## 2.2. Photocatalysis

10mg/L Rhodamine B (RhB) solution as a testing organics pollutant was prepared. Take the four annealed samples 60mg each to grind in 0.5mL acetic acid and 2ml deionized water respectively for four types of uniformly-disperse mixtures. Afterwards, these four mixtures were added to four 60ml RhB solutions respectively for photocatalytic decomposition of RhB in a UV lamp. The photocatalytic decomposition reactions were proceeding at 40°C ( $\pm 2^\circ\text{C}$  error) with magnetic stirring. During the whole reaction, about 4mL liquids were extracted at a given time intervals and subsequently the catalysts were separated from the extracted liquids by centrifugation. The supernatants were analyzed by recording the variations of RhB absorption band by a TU-1901 spectrophotometer.

## 2.3. Characterization

The morphologies of the samples were characterized by field-emission scanning electron microscopy (SEM) (Hitachi S-4800) and transmission electron microscope (TEM) (FEI Tecnai F30). Grazing-angle XRD (Philips, X'Pert Pro, Cu K $\alpha$ 1, 1.54056 Å, 1°) were employed for structure analysis. The ultraviolet-visible (UV-Vis) absorption spectra of the samples were recorded using a TU-1901 spectrophotometer.

## 3. Results and Discussion

Fig. 1 shows the SEM images of anodized TiO<sub>2</sub> nanotube without and with different Fe-doped amounts. Fig. 1a presents the typical morphology of the anodized TiO<sub>2</sub> nanotube after grinding and sintering process. The randomly-oriented nanotubes and nanoparticles in Fig. 1a show a smooth and clean surface. Fig. 1b, Fig. 1c, and Fig. 1d show anodized TiO<sub>2</sub> nanotube with different of Fe-doped amounts named as Fe-0.05-TiO<sub>2</sub>, Fe-0.1-TiO<sub>2</sub>, Fe-0.2-TiO<sub>2</sub>. It can be seen from Fig. 1b-d, the morphologies of nanotubes transit from smooth-type to granular-type as the Fe-ions contents increases. Meanwhile, the grains consisting of nanotubes grow larger with the increased Fe-ions content and reach the maximum in sample of Fe-0.1-TiO<sub>2</sub>. To be accompanied by, the diameters of nanotubes grow larger with the diameter grow from 50 nm to 100 nm.

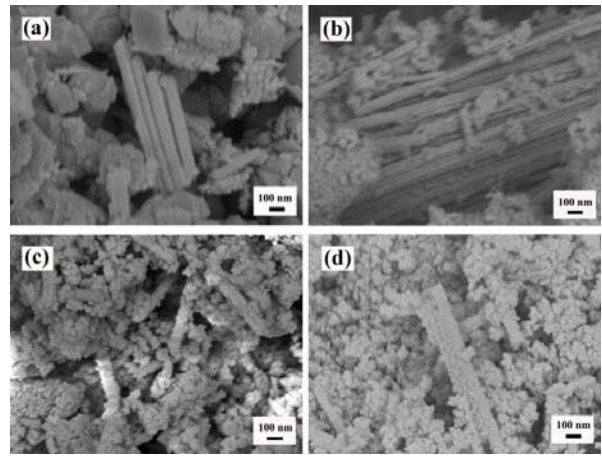


Fig. 1. SEM images of anodized TiO<sub>2</sub> nanotube with different Fe-doped amounts: undoped TiO<sub>2</sub>(a), Fe-0.05-TiO<sub>2</sub>(b), Fe-0.1-TiO<sub>2</sub>(c), Fe-0.2-TiO<sub>2</sub>(d) after grinding and sintering.

The TEM images of the anodized TiO<sub>2</sub> nanotube without and with different Fe-doped amounts are shown in Fig. 2. From Fig. 2a, the undoped TiO<sub>2</sub> nanotubes present a smooth structure and display a diameter of about 50 nm with a transparent and uniform-size morphology. Fig. 2b, Fig. 2c, and Fig. 2d show the morphologies of Fe-doped nanotubes with different Fe-doped amounts: Fe-0.05-TiO<sub>2</sub>, Fe-0.1-TiO<sub>2</sub>, Fe-0.2-TiO<sub>2</sub>, which all display granular-type morphology. They all present nanotube and nanoparticle composite structure consists of even smaller grains about 20-30 nm. There is a gradual change that the diameter of nanotube grows larger as the increase of Fe-doped content.

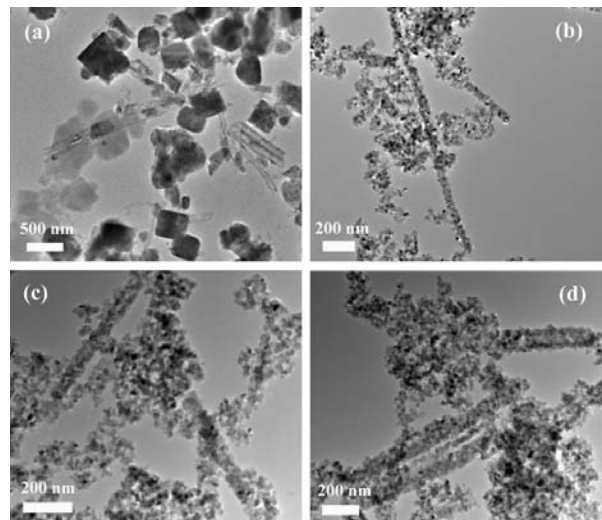


Fig. 2. TEM images of anodized TiO<sub>2</sub> nanotube with different Fe-doped amounts: undoped TiO<sub>2</sub>(a), Fe-0.05-TiO<sub>2</sub>(b), Fe-0.1-TiO<sub>2</sub>(c), Fe-0.2-TiO<sub>2</sub>(d) after grinding and sintering.

Fig. 3 shows the XRD patterns of the undoped and Fe-doped TiO<sub>2</sub> nanotube with Fe-doped amounts increase. The observed peaks, can be assigned to the (101), (004), and (200) etc. as marked in Fig. 3, reflect different crystalline plan of anatase phase of TiO<sub>2</sub> materials (PDF#211272). However, no other XRD peaks are corresponded for other crystalline phase of TiO<sub>2</sub> or relevant phase of Fe oxide forms. XRD analysis indicates that all the nanotubes and nanoparticles are predominantly of polycrystalline ananase structure, in despite of the Fe dopants. Further observations find that there is a shift to a larger angle of diffraction peak of Fe-0.1-TiO<sub>2</sub> nanotube compared to that of the undoped nanotube, as shown in the inset of Fig. 3. The shift of (101) peak between the two samples was found to be 0.03°. The small shift could be attributed to the larger atom radius of substituted Fe<sup>3+</sup> (0.64 Å) than that of Ti<sup>4+</sup> (0.605 Å) in the polycrystalline lattice. The shift of the diffraction peak verifies that Fe has been incorporated into the TiO<sub>2</sub> lattice.

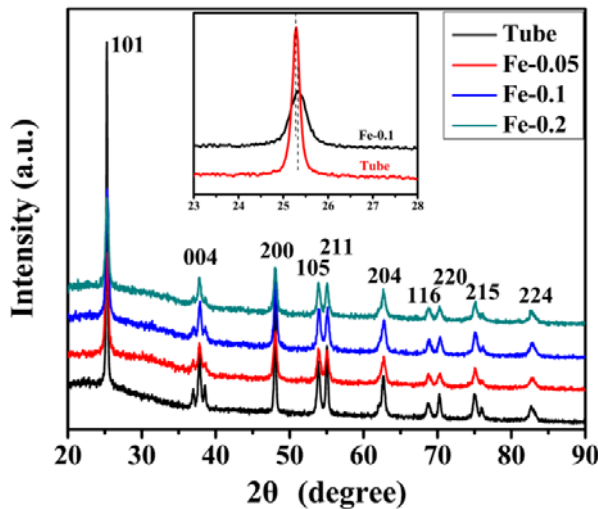


Fig. 3. XRD patterns of undoped and Fe-doped TiO<sub>2</sub> nanotubes with different Fe-doped amounts annealed at 550 °C in air. The inset indicates the shift of the (101) peak between the undoped TiO<sub>2</sub> nanotube and Fe-0.1-TiO<sub>2</sub> nanotube.

The average crystallize sizes of all the samples can be estimated from the most prominent (101) peak of the XRD patterns by Scherrer formula, expressed as

$$D = \frac{0.89\lambda}{\beta \cos\theta} \quad (1)$$

where D, λ, θ, and β are the mean crystallize sizes, the wavelength of X-ray corresponding to the Cu Ka radiation, Bragg diffraction angle, and the full width at half maximum of the diffraction peak, respectively. The crystallite sizes of all the samples can be calculated as shown in Table 1. The data shows that the incorporation of

Fe into TiO<sub>2</sub> nanotube could lead to a greatly decrease of the crystallize size. This reflects as a large morphology transform that from smooth nanotube to granular-type nanotube, as verified in Fig. 1 and Fig. 2. The three types of Fe-doped nanotubes present a similar crystallize size reflecting a similar structure.

Table 1. The crystal sizes and weight percentages of Fe contents of the four samples.

Sample	Crystallize size (nm) <sup>a</sup>	Fe content (wt%) <sup>b</sup>
Undoped TiO <sub>2</sub>	49.8	0
Fe-0.05-TiO <sub>2</sub>	22.4	0.073
Fe-0.1-TiO <sub>2</sub>	24.5	0.091
Fe-0.15-TiO <sub>2</sub>	23.4	0.094

<sup>a</sup> Calculated by Scherrer formula:  $D = \frac{0.89\lambda}{\beta \cos\theta}$ ,  $\theta=25.3$ ,  $\lambda=0.15406$  nm.

<sup>b</sup> Obtained from Inductive Coupled Plasma Emission Spectrometer.

Meanwhile, the precise contents of Fe in different samples can be obtained from the inductive coupled plasma emission spectrometer (ICP). The ICP results are also listed in Table 1. It demonstrates that the actual content of Fe increases but increases slower with the increased Fe(NO<sub>3</sub>)<sub>3</sub> amount in the solution, indicating that Fe-ions in the solution has been deposited on the surface of TiO<sub>2</sub> but the doped amount is limited.

The absorption curves of the extracted solution are displayed in Fig. 4. They reflect the concentration variations of RhB by recording a characteristic absorption peak (554 nm) of RhB in the UV–Vis spectrum. Fig. 4a, Fig. 4b, Fig. 4c, and Fig. 4d show the variations of the RhB absorption peaks with catalysts of Fe-0.05-TiO<sub>2</sub>, Fe-0.1-TiO<sub>2</sub>, Fe-0.2-TiO<sub>2</sub> and undoped TiO<sub>2</sub> under different exposure time, respectively. The corresponding RhB concentration evolutions to irradiation time are presented in Fig. 4e. The results show that Fe-0.1-TiO<sub>2</sub> nanotubes as catalyst present better photocatalytic efficiency than Fe-0.05-TiO<sub>2</sub> or Fe-0.2-TiO<sub>2</sub> Fe-doped TiO<sub>2</sub> nanotube. Further comparing the variations of the absorption peaks of the pure and Fe-doped samples indicate that only Fe-0.1-TiO<sub>2</sub> nanotubes perform better photocatalytic activity than the undoped TiO<sub>2</sub> nanotubes. While Fe-0.05-TiO<sub>2</sub> nanotubes show comparative photocatalytic activity with the undoped TiO<sub>2</sub> nanotube. More amounts of Fe-doped nanotubes such as Fe-0.2-TiO<sub>2</sub> nanotube would decrease the photo-decomposition activity of catalyst.

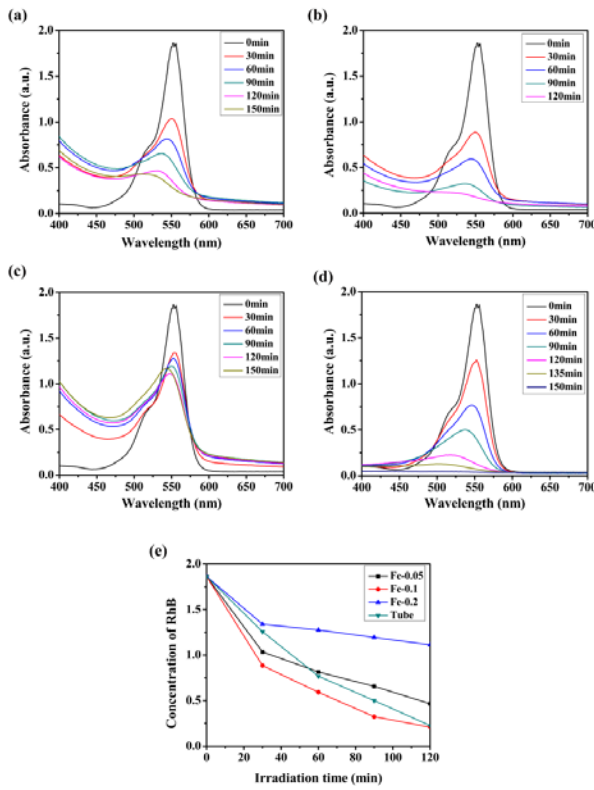
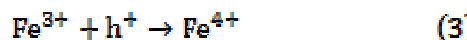


*Fig. 4. Absorption curves of RhB solution under UV light irradiation of catalyst Fe-0.05-TiO<sub>2</sub>(a), Fe-0.1-TiO<sub>2</sub>(b), Fe-0.2-TiO<sub>2</sub>(c) and undoped TiO<sub>2</sub>(d). The concentration of RhB (from the optical absorbance measurements at 554 nm) with four different photocatalyst in the solution versus the exposure time under UV irradiation reflect as Fig. 4(e).*

Previous researches have demonstrated that TiO<sub>2</sub> band gap energy can reduce when Fe is doped into TiO<sub>2</sub> lattice [22, 23], which made it more easy for catalyst to absorb visible and nearly ultraviolet light to induce electron-hole pair generation. This implies that more Fe-doped amounts would produce more photocatalytic activity. However, it is confirmed in our experiment that only optimal Fe-doped contributes to photocatalytic activity, Fe-doping too little or too much would prevent photocatalytic activity.



From the above two formulas (2)-(3), as the increment of Fe-doped amounts, the doped-Fe ions could play a role as electron trap (2) or hole traps (3), the electron transits from conduction band of TiO<sub>2</sub> to Fe<sup>3+</sup>/Fe<sup>2+</sup> band and hole

transits from valence band of TiO<sub>2</sub> to Fe<sup>4+</sup>/Fe<sup>3+</sup> band and then store electron or hole in Fe<sup>3+</sup> and converts Fe<sup>3+</sup> to Fe<sup>2+</sup> or Fe<sup>3+</sup> to Fe<sup>4+</sup>, respectively. And then release e<sup>-</sup>/h<sup>+</sup> couple in the photodecomposition process gradually. The electron and hole transferring process are displayed as Fig. 5. The e<sup>-</sup>/h<sup>+</sup> storage reduce e<sup>-</sup>/h<sup>+</sup> pair recombination rate [23, 24], which is favorable for light catalytic efficiency. Therefore, when the Fe-doped amount is lower than a optimal value, the increased e<sup>-</sup>/h<sup>+</sup> pairs could not produce sufficient e<sup>-</sup>/h<sup>+</sup> pair for photocatalytic efficiency. However, when the Fe-doped amount excess than optimal value, Fe-ions would act as electron or hole recombination center instead of storage center, which decrease photocatalytic efficiency immensely.

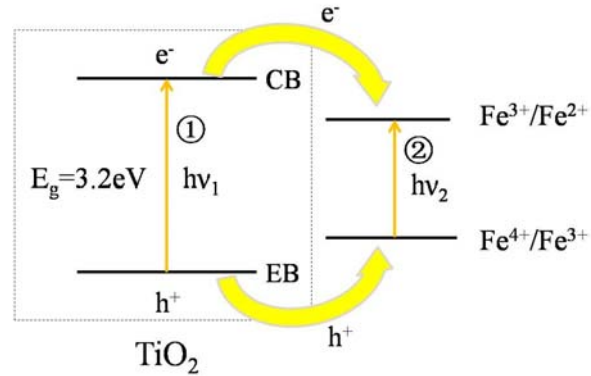


*Fig. 5. Schematic illustration of electron or hole transfer and the role of Fe<sup>3+</sup> as electron or hole traps*

#### 4. Conclusions

Fe-doped TiO<sub>2</sub> nanotubes have been synthesized successfully by anodization and solution-coating technique. SEM and TEM images both verified the structural evolution from smooth-type TiO<sub>2</sub> nanotube to granular-type Fe-doped TiO<sub>2</sub> nanotube. The data from ICP and the shift of (101) peak in XRD patterns confirm Fe-ions has been incorporated into the TiO<sub>2</sub> lattice. The photo-decomposition efficiency comparisons of RhB solution with the four-type catalysts indicate that Fe-doped TiO<sub>2</sub> nanotubes with a optimal concentration would improve photocatalytic efficiency than undoped TiO<sub>2</sub> or Fe-doped TiO<sub>2</sub> in small quantity as catalysts. This could be explained as Fe-ions may play a role as e<sup>-</sup> or h<sup>+</sup> traps and reduces e<sup>-</sup>/h<sup>+</sup> pair recombination rate for light catalytic process. However, excessive Fe-doped amounts would decreases photocatalytic efficiency as well. This should be attributed to the excessive Fe-ions acting as electron or hole recombination center instead.

### Acknowledgements

This work is supported by Scientific research plan projects of Education Department of Shaanxi province of China (Grant No. 12JK0983), Natural Science Basic Research plan in Shaanxi Province of China (Grant No. 2012JQ1011) and Key project of Baoji university of arts and science (Grant No. ZK12047).

### References

- [1] J. Kim, W. Choi, *Appl. Catal. B: Environ.* **106**, 39 (2011).
- [2] S. H. Hwang, C. Kim, J. Jang, *Catal. Commun.* **12**, 1037 (2011).
- [3] W. K. Oh, S. Kim, M. Choi, C. Kim, Y. S. Jeong, B. R. Cho, J. S. Hahn, J. Jang, *Acs Nano* **4**, 5301 (2010).
- [4] D. Kuang, J. Brillet, P. Chen, M. Takata, S. Uchida, H. Miura, K. Sumioka, S. M. Zakeeruddin, M. Grätzel, *Acs Nano* **2**, 1113 (2008).
- [5] Z. Liu, X. Yan, W. Chu, D. Li, *Appl. Surf. Sci.* **257**, 1295 (2010)
- [6] J. M. Macak, M. Zlamal, J. Krysa, P. Schmuki, *Small* **3**, 300 (2007).
- [7] A. B. F. Martinson, J. W. Elam, J. T. Hupp, M. J. Pellin, *Nano Lett.* **7**, 2183 (2007).
- [8] D. Wang, B. Yu, F. Zhou, C. Wang, W. Liu, *Mater. Chem. Phys.* **113**, 602 (2009).
- [9] W. Lee, J. Lee, S. K. Min, T. Park, W. Yi, S. H. Han, *Mater. Sci. Eng. B* **156**, 48 (2009).
- [10] B. A. Lu, X. D. Li, T. H. Wang, E. Q. Xie, Z. Xu, *J. Mater. Chem. A* **1**, 3900 (2013).
- [11] Z. Liu, X. Zhang, S. Nishimoto, M. Jin, D. A. Tryk, T. Murakami, A. Fujishima, *J. Phys. Chem. C* **112**, 253 (2008).
- [12] D. J. Yang, H. Park, S. J. Cho, H. G. Kim, W. Y. Choi, *J. Phys. Chem. Solids* **69**, 1272 (2008).
- [13] M. Paulose, K. Shankar, S. Yoriya, H. E. Prakasam, O. K. Varghese, G. K. Mor, T. A. Latempa, A. Fitzgerald, C. A. Grimes, *J. Phys. Chem. B* **110**, 16179 (2006).
- [14] A. Fujishima, T. N. Rao, D. A. Tryk, *J. Photochem. Photobiol. C* **1**, 1 (2000).
- [15] E. J. Wolfrim, J. Huang, D. M. Blake, P. Maness, Z. Huang, J. Fiest, *Environ. Sci. Technol.* **36**, 3412 (2002).
- [16] C. Hu, J. C. Yu, Z. Hao, P. K. Wong, *Appl. Catal. B: Environ.* **42**, 47 (2003).
- [17] G. H. Zhang, H. G. Duan, B. A. Lu, Z. Xu, *Nanoscale* **5**, 5801 (2013).
- [18] L. Li, H. S. Zhuang, D. Bu, *Appl. Surf. Sci.* **257**, 9221 (2011).
- [19] Y. D. Hou, X. C. Wang, L. Wu, X. F. Chen, Z. X. Ding, X. X. Wang, X. Z. Fu, *Chemosphere*, **72**, 414 (2008).
- [20] W. Tang, X. Chen, J. Xia, J. Gong, X. Zeng, *Mater. Sci. Eng. B* **187**, 39 (2014).
- [21] S. George, S. Pokhrel, Z. Ji, B. L. Henderson, T. Xia, L. J. Li, J. I. Zink, A. E. Nel, L. Mädler, *J. Am. Chem. Soc.* **133**, 11270 (2011).
- [22] H. Yamashita, M. Haraa, J. Misaka, M. Takeuchi, B. Neppolian, M. Anpo, *Catal. Today* **84**, 191 (2003).
- [23] Y. Zhang, Y. Shen, F. Gu, M. M. Wu, Y. Xie, J. C. Zhang, *Appl. Surf. Sci.* **256**, 85 (2009).
- [24] J. Zhu, W. Zheng, B. Hea, J. Zhang, M. Anpo, *J. Mol. Catal. A* **216**, 35 (2004).

\*Corresponding author: kangcp06@126.com